

# Discrete Breathers in Two-Dimensional Anisotropic Nonlinear Schrödinger lattices

J. Gómez-Gardeñes<sup>a,b,c</sup>, L.M. Floría<sup>a,b,c</sup> and A.R. Bishop<sup>d</sup>

<sup>a</sup>*Dpt. de Física de la Materia Condensada, Universidad de Zaragoza, 50009 Zaragoza, Spain.*

<sup>b</sup>*Dept. de Teoría y Simulación de Sistemas Complejos, Instituto de Ciencia de Materiales de Aragón (ICMA), C.S.I.C.-Universidad de Zaragoza, 50009 Zaragoza, Spain.*

<sup>c</sup>*Instituto de Biocomputación y Física de Sistemas Complejos (BIFI), Universidad de Zaragoza, Zaragoza 50009, Spain*

<sup>d</sup>*Theoretical Division and Center for Nonlinear Studies, Los Alamos National Laboratory, Los Alamos, New Mexico 87545*

---

## Abstract

We study the structure and stability of discrete breathers (both pinned and mobile) in two-dimensional nonlinear anisotropic Schrödinger lattices. Starting from a set of identical one-dimensional systems we develop the continuation of the localized pulses from the weakly coupled regime (strongly anisotropic) to the homogeneous one (isotropic). Mobile discrete breathers are seen to be a superposition of a localized mobile core and an extended background of two-dimensional nonlinear plane waves. This structure is in agreement with previous results on one-dimensional breather mobility. The study of the stability of both pinned and mobile solutions is performed using standard Floquet analysis. Regimes of quasi-collapse are found for both types of solutions, while another kind of instability (responsible for the discrete breather fission) is found for mobile solutions. The development of such instabilities is studied examining typical trajectories on the unstable nonlinear manifold.

*Key words:*

*PACS:* 05.45.–a, 63.20.Pw

---

---

*Email address:* [gardenes@unizar.es](mailto:gardenes@unizar.es) (J. Gómez-Gardeñes).

## 1 Introduction

We present a numerical study of exact breather dynamics in two-dimensional nonlinear Schrödinger lattices. This issue fits well with the enduring scientific interests of Serge Aubry in the many faceted subject of localization and transport in nonlinear macroscopic discrete systems, where Serge's outstanding contributions are widely recognized. Many ideas and lines of study followed in the investigation reported here have found a source of inspiration in early works of Aubry and collaborators, among which the doctoral works of Th. Cretegny and J.L. Marín deserve special mention.

The existence and properties of localized solutions in extended discrete systems have attracted interest in a broad range of physical fields [1]. Discrete breathers, sometimes referred to as intrinsic localized modes, are spatially localized and time periodic solutions. These solutions arise in the context of nonlinear discrete systems and are of fundamental interest for varied physical applications such as pulse propagation in nonlinear optics, energy storing and transport in biomolecules, plasma physics, etc... The existence of discrete breathers in these systems has been proved rigorously [2] for a number of equations with physical relevance and, contrary to continuous nonlinear equations, their existence can be regarded as a generic feature of these systems. One of the most important class of equations are the so-called *discrete nonlinear Schrödinger lattices* [3,4]. The existence of discrete breathers has been proven for a wide range of systems belonging to this class of nonlinear difference-differential equations. In particular, the most important example of wide applicability is the standard nonlinear Schrödinger equation. For instance, this equation was employed in [6,7] for describing the propagation of localized beams in an array of nonlinear (Kerr type) waveguides, having experimental validation subsequently reported in [8,9].

The study of two-dimensional nonlinear Schrödinger lattices has attracted much attention [10,11] in recent years due to the new phenomena emerging when the dimensionality of the lattice is increased. Some examples of these new features are the existence of vortex-breathers [12] which supports energy flux, the appearance of an energy threshold for the creation of discrete breathers [13,14,15,16,17] and the ubiquity of an instability (the quasi-collapse) of some discrete breather solutions leading to a highly localized pulson state [18,19,20,?,22,23]. These theoretical efforts have their counterpart in recent advances in the field of nonlinear optics. The studies of two-dimensional arrays of coupled nonlinear waveguides allow the experimental observation of those effects studied theoretically. Specially relevant is the recent experimental breakthrough (theoretically designed in [24]) by Fleisher *et al* [25,26], where a two-dimensional array of nonlinear waveguides is induced in a photosensitive material. This technique provides a clear experimental verification of the two-

dimensional discrete breather existence in this system. In particular, besides the observation of standard discrete breathers, these works reported the first observations of staggered discrete breathers.

Our study here will focus on the computation of numerically exact discrete breathers in two-dimensional anisotropic nonlinear Schrödinger lattices, *i.e.* where the couplings in the two spatial directions are different. The use of shooting methods allow us to find these solutions and analyze their structural and stability properties. Both pinned and mobile discrete breathers are studied. In the latter case we will study only the ones whose motion is along one axis of the lattice. The analysis of the numerically exact solutions shed light on some features of the properties and stability of localized solutions reported in previous works.

The plan of the paper is as follows: In section 2 we provide the technical background and details needed for self-contained purposes. First we summarize in 2.1 the main conclusions on the dynamics of 1D Schrödinger discrete breathers reported in [27,28]. A detailed account of the numerical methods (SVD-regularized Newton continuation of operator fixed points) that we have used can be found in that reference. Also in 2.1, we discuss briefly the most relevant formal differences with respect to alternative approaches to (one-dimensional) exact mobility of discrete breathers, *e.g.* those in refs [29] and [30,31]. In subsection 2.2 we introduce the two-dimensional anisotropic Salerno lattice and provide explanations on the implementation of the numerical procedures used to study the dynamics of 2D discrete breathers.

The analysis of the results of our numerics on pinned discrete breathers for anisotropic nonlinear Schrödinger lattices is reported in section 3. We present the numerical computations of the fixed point norm, as a function of three parameters: breather frequency, transversal coupling, and nonlinearity (see below). They show, as anticipated, the so-called *quasi-collapse* transition, associated with the (well-known) existence of thresholds for the breather norm in two-dimensional lattices. We present numerically computed sectors of the bifurcation surface. We conclude this section with a brief look at the nonlinear dynamics on the unstable manifold, whose typical trajectories have been called *pulson* states. Early numerical work on the 2D quasi-collapse phenomena in isotropic lattices was reported in [22,23] and [20]. A two-year-old account of the "state of knowledge" on 2D Schrödinger lattices can be found in Section six of [3].

In section 4 we show results on a type of mobile breather, namely those moving along the direction of stronger lattice coupling constant. The structure of each of these mobile exact discrete breathers is that of a localized moving *core* superimposed on a specific extended state of resonant small amplitude radiation, the *background*. We present here the results of an extensive Floquet sta-

bility analysis of this type of solutions in two sectors of the three-dimensional parameter space, which clearly show the existence of two different transitions. The tangent space eigenvectors associated to each of the transitions are presented, and the relation of the unstable manifold trajectories to pulson states is analyzed afterwards.

We conclude with section 5, where we briefly review the results obtained and illustrate their possible implications for mobility of 2D discrete breathers.

## 2 Numerical continuation and preliminary results

The use of numerical tools for the continuation of discrete breather solutions has been widely employed since their existence proof was reported (see *e.g.* [32,33]). In particular, the design of numerical techniques for finding exact mobile breathers based on those employed for the pinned ones has been explored in the recent years [27,28,34,35,36] and paves the way to resolving the still open question about discrete breather mobility. Here, after reviewing the most important features of 1D mobile breathers in nonlinear Schrödinger lattices, we briefly explain how the continuation method is implemented in our system.

### 2.1 Mobility of one-dimensional nonlinear Schrödinger discrete breathers

As was introduced in section 1, exact mobility of discrete breathers in 1D Schrödinger nonlinear lattices were numerically studied by the authors in previous works [27,28]. In particular, a numerical continuation from the integrable *Ablovitz-Ladik lattice*, A-L, (where exact mobile breathers can be calculated analytically [37]),

$$i\dot{\Phi}_n = -(\Phi_{n+1} + \Phi_{n-1}) \left[ 1 + \frac{\gamma}{2} |\Phi_n|^2 \right], \quad (1)$$

to the standard *discrete nonlinear Schrödinger equation*, DNLS,

$$i\dot{\Phi}_n = -(\Phi_{n+1} + \Phi_{n-1}) - \gamma |\Phi_n|^2 \Phi_n, \quad (2)$$

was performed within the so-called *Salerno model* [38],

$$i\dot{\Phi}_n = -(\Phi_{n+1} + \Phi_{n-1}) \left[ 1 + \mu |\Phi_n|^2 \right] - 2\nu \Phi_n |\Phi_n|^2, \quad (3)$$

where  $\gamma$ ,  $\mu$  and  $\nu$  are the parameters accounting for the strength of the non-linear terms. The above equation includes the former two relevant equations (1) and (2), for  $(\mu = \gamma/2, \nu = 0)$  and  $(\mu = 0, \nu = \gamma/2)$  respectively, providing the desired interpolation needed to develop the continuation scheme. The integrability of equation (1) provides for  $\gamma > 0$  a two-parametric family of discrete breathers

$$\Phi_n(t) = \sqrt{\frac{2}{\gamma}} \sinh\beta \operatorname{sech}[\beta(n - x(t))] \exp[i(\alpha(n - x(t)) - \Omega(t))], \quad (4)$$

where the two parameters  $\alpha \in [-\pi : \pi]$  and  $\beta > 0$  describe the velocity and internal frequency of the solution

$$v_b = \dot{x} = 2 \sinh\beta \sin\alpha / \beta, \quad (5)$$

$$\omega_b = \dot{\Omega} = 2 \cosh\beta \cos\alpha + \alpha v_b. \quad (6)$$

The Salerno lattice (3), possess two dynamical invariants, namely the hamiltonian,

$$\begin{aligned} \mathcal{H} = & - \sum_n (\Phi_n \bar{\Phi}_{n+1} + \bar{\Phi}_n \Phi_{n+1}) - 2 \frac{\nu}{\mu} \sum_n |\Phi_n|^2 \\ & + 2 \frac{\nu}{\mu^2} \sum_n \ln(1 + \mu |\Phi_n|^2), \end{aligned} \quad (7)$$

where  $\bar{\Phi}_n$  denotes the complex conjugate of  $\Phi_n$ , and the norm

$$\mathcal{N} = \frac{1}{\mu} \sum_n \ln(1 + \mu |\Phi_n|^2). \quad (8)$$

In order to find exact mobile discrete breathers in the Salerno model we define a  $(p, q)$ -resonant solution  $\Phi_n(t)$  referred to some time scale  $\tau$  such that

$$\Phi_n(t_0) = \Phi_{n+p}(t_0 + q\tau). \quad (9)$$

Within the above definition, a mobile breather that translates  $p$  sites after  $q$  periods of the internal oscillation will satisfy equation (9) when  $\tau = T_b$ . In this sense, the continuation focuses on the families of  $(p, q)$ -resonant discrete breathers, that is breather solutions with the two characteristic time scales (corresponding to the breather velocity,  $v_b$ , and the internal frequency,  $\omega_b$ ) being commensurate. In all the computations we have used finite lattices with periodic boundary conditions (PBC) so that  $\Phi_{N+1} = \Phi_1$  and  $\Phi_0 = \Phi_N$  (with  $N$  being the lattice size).

In the previous works [27,28] the authors start from those A-L solutions which are  $(p, q)$ -resonant, we discretize (fine grid) the path  $\mu + \nu = 1$  (with  $\mu$  and  $\nu$  being positive) along the Salerno model, and go through it computing the corresponding  $(p, q)$ -resonant solutions for the pairs  $(\mu, \nu)$ . We can choose the path without loss of generality because of the scaling property of equation (3). Then, each solution is numerically computed as a fixed point of the map

$$M = L^p T_{(\omega_b, \nu)}^q, \quad (10)$$

where  $L$  is the lattice translation operator  $L(\{\Phi_n(t_0)\}) = \{\Phi_{n+1}(t_0)\}$ , and  $T_{(\omega_b, \nu)}$  is the  $T_b$ -evolution map ( $T_b = 2\pi/\omega_b$ ) following the dynamics dictated by equation (3) for the corresponding value of  $\nu$  ( $\mu = 1 - \nu$ ); *i.e.*,  $T_{(\omega_b, \nu)}[\{\Phi_n(t_0)\}] = \{\Phi_n(t_0 + T_b)\}$ .

The continuation was then performed for a fine grid of frequencies belonging to the family of  $(p = 1, q = 1)$ -resonant discrete breathers. The most important conclusion about discrete breathers in these nonlinear Schrödinger lattices is that mobility in the non-integrable regime ( $\nu \neq 1$ ) demands the presence of an extended *background* to which the fixed point solution is spatially asymptotic ( $n \rightarrow \infty$ ), *i.e.* the solution is exactly written as

$$\Phi_n(t) = \Phi_n^{\text{core}}(t) + \Phi_n^{\text{bckg}}(t). \quad (11)$$

This expression defines the purely localized component  $\Phi_n^{\text{core}}(t)$  of the solution. The background is a finite linear combination of nonlinear plane waves,  $\Phi_n^{\text{bckg}}(t) = \sum_{j=1}^s A_j \exp[i(k_j n - \omega(k_j, A_j)t)]$ . These plane waves are exact solutions of the Salerno model (3) being the nonlinear dispersion relation  $\omega(k_j, A_j) = -2[1 + \mu|A_j|^2] \cos k_j - 2\nu|A_j|^2$ . The results concerning the characterization of the background are discussed in detail in [27,28], here we briefly summarize the most important features:

- (i) The set of “ $s$ ” plane waves which take part in the background of a  $(p, q)$ -resonant discrete breather with internal frequency  $\omega_b$  is derived by the simple selection rule for the wave-numbers  $k_j$

$$\frac{\omega(k_j, A_j)}{\omega_b} = \frac{1}{q} \left( \frac{p}{2\pi} k_j - m \right), \quad (12)$$

*i.e.* only the plane waves which are  $(p, q)$ -resonant with the internal period of the breather can be components of  $\{\Phi_n^{\text{bckg}}(t)\}$ . The number of solutions of (12) fixes “ $s$ ”.

- (ii) The amplitudes  $\{A_j\}$  of the nonlinear plane waves differ by orders of magnitude.

- (iii) There exist a strong positive correlation between the amplitude of the background and the strength of the Peierls-Nabarro barrier arising from the periodic lattice. This correlation is particularly clear when symmetry breaking transitions occur for the also studied case of  $\nu < 0$  and  $\mu > 0$  (see reference [28]), and reflects the link between non-integrability and the existence of the background dressing of the mobile core.
- (iv) Finally, the interpretation of the correlation described in (iii) is reinforced from a study of the energy evolution of the mobile core: *There is an energy balance brought by the background when the core moves along the lattice.* In particular, it can be observed how the core energy oscillates periodically so that it takes the maximum energy value when the core visits the inter-site configuration. This extra energy periodically obtained by the core is provided by the background, with the energy maximum clearly related to the background amplitude.

Before concluding this subsection, it is worth commenting on some of the differences between the Newton continuation of fixed points that we use in this paper, and other important recent approaches to breather numerics. The work by Ablowitz *et al* [29] uses discrete Fourier analysis to obtain a nonlinear non-local integral equation, from where the " ... soliton is thus viewed as a fixed point of a nonlinear functional" (sic) in the Fourier transformed space of functions. Following these authors, their results seem to differ from those of early pioneering work [39] (nowadays textbook material [1]) "in which a *continuous* travelling solitary waves were reported using Fourier series expansions with finite period  $L$  while assuming convergence as  $L \rightarrow \infty$ " (sic). Ablowitz *et al* term *continuous* a solution that can be defined off the lattice points, which they see as "necessary when discussing travelling waves in lattices" (sic), and disagree with some conclusions reported in the earlier works.

The ("orthodoxy matters") discussion above helps us to clarify how differently our numerical approaches "sees" the discrete Schrödinger breather problem: The very concept of a variable defined off the lattice points is intrinsically alien to our discrete approach, which neither needs of it nor excludes its eventual consideration. In contrast to those views (but not at all in logical opposition), we consistently view the thermodynamical limit ( $N \rightarrow \infty$ ) in lattice space, much in the sense used *e.g.* by Serge Aubry in his celebrated work on the Frenkel-Kontorova ground state problem [40]: The infinite size limit is built up from a subsequence of PBC (finite) lattices for which the limit is well defined. This will make the Fourier-transformed  $k$ -space continuum.

Closer to our approach in some respects, though technically different in many others, is the formal approach purposed recently by James and collaborators [30,31]. This approach, which uses recent central manifold theorems, was brought to our attention very recently and unfortunately, we have to defer to a future publication a comparison of our 1D computations with theirs, this

is beyond the scope of this paper, namely, the anisotropic 2D Schrödinger lattices, which we introduce in the next subsection.

## 2.2 Two-dimensional anisotropic lattices.

Motivated by the method described above, we can extend the continuation scheme for calculating exact discrete breathers in higher dimensional systems. In particular we focus on the two-dimensional nonlinear Schrödinger lattice

$$\begin{aligned} i\dot{\Phi}_{nm} = & -C_1(\Phi_{n+1,m} + \Phi_{n-1,m})(1 + \mu|\Phi_{n,m}|^2) \\ & -C_2(\Phi_{n,m+1} + \Phi_{n,m-1})(1 + \mu|\Phi_{n,m}|^2) \\ & -2\nu\Phi_{n,m}|\Phi_{n,m}|^2. \end{aligned} \quad (13)$$

This lattice can be viewed as the *two-dimensional Salerno model*. The two coupling parameters  $C_1$  and  $C_2$  provide a technical advantage for numerics (see below), but they are also introduced for theoretical and experimental interest. The possibility of controlling the ratio between the two linear couplings of the two transversal directions has been studied in various works as a way of analysing how the intrinsic 2D phenomena (such as the quasi-collapse) emerge. In fact, for  $C_1 \ll C_2$ ,  $\mu = 0$  and  $\nu = \gamma/2$  equation (13) describes a set of weakly coupled nonlinear waveguide arrays and can be considered as a case of “*intermediate dimensionality*”. This extreme has been studied experimentally in [41] and using perturbative methods in [42]. On the other hand, this equation incorporates, as two particular limits, the physically relevant standard two-dimensional DNLS equation ( $\mu = 0$ ,  $\nu = \gamma/2$ ) and the two-dimensional A-L lattice ( $\mu = \gamma/2$ ,  $\nu = 0$ ). The continuation between these two limits provides a useful tool for studying the interplay between the on-site and inter-site nonlinearity in the 2D anisotropic lattice. Moreover, the anisotropy (or freedom in the values of the coupling parameters  $C_1$  and  $C_2$ ) allows to include an integrable model among the members of the family of nonlinear lattices described by (13). That is, for  $\nu = 0$ ,  $C_i = 0$  and  $C_j \neq 0$  one obtains a set of integrable A-L chains. In this way, every 2D model included in (13) is connected with an integrable model where analytic discrete breathers are available. In what follows we set  $\gamma = 2$  and  $\nu = 1 - \mu$  with  $\nu > 0$  and  $\mu > 0$ .

The dynamics (13) can be derived from the Salerno Poisson structure

$$\{\mathcal{A}, \mathcal{B}\} = \sum_{n,m} \left( \frac{\partial \mathcal{A}}{\partial \Phi_{n,m}} \frac{\partial \mathcal{B}}{\partial \bar{\Phi}_{n,m}} - \frac{\partial \mathcal{A}}{\partial \bar{\Phi}_{n,m}} \frac{\partial \mathcal{B}}{\partial \Phi_{n,m}} \right) \cdot (1 + \mu|\Phi_{n,m}|^2), \quad (14)$$

with the hamiltonian

$$\begin{aligned}
\mathcal{H} = & -C_1 \sum_{n,m} \left( \Phi_{n,m} \bar{\Phi}_{n+1,m} + \Phi_{n+1,m} \bar{\Phi}_{n,m} \right) \\
& -C_2 \sum_{n,m} \left( \Phi_{n,m} \bar{\Phi}_{n,m+1} + \Phi_{n,m+1} \bar{\Phi}_{n,m} \right) \\
& - \frac{2\nu}{\mu} \sum_{n,m} |\Phi_{n,m}|^2 + \frac{2\nu}{\mu^2} \sum_{n,m} \ln \left( 1 + \mu |\Phi_{n,m}|^2 \right) .
\end{aligned} \tag{15}$$

As in the 1D Salerno model there is also a second conserved quantity, the norm, due to the phase invariance of the equations of motion (13)

$$\mathcal{N} = \frac{1}{\mu} \sum_{n,m} \ln \left( 1 + \mu |\Phi_{n,m}|^2 \right) . \tag{16}$$

In the same manner as in the 1D case we will focus on a special set of 2D discrete breathers. For this, we have to generalize the definition (9) of a resonant solution in the two-dimensional case. In this context discrete breather solutions are characterized by three time scales. Namely, one associated with the internal oscillation  $\omega_b$  and the other two derived from the translation of the localization center, *i.e.* its velocity  $\vec{v}_b = (v_x, v_y)$ . The subset of 3-tuples  $(\omega_b, \vec{v}_b)$  that fulfil the  $(p_x, p_y, q)$ -resonance condition

$$v_x \frac{2\pi}{\omega_b} = \frac{p_x}{q} \tag{17}$$

$$v_y \frac{2\pi}{\omega_b} = \frac{p_y}{q} , \tag{18}$$

(where  $p_x$ ,  $p_y$  and  $q$  are integers) denote the breather solution that can be obtained with our continuation method. These solutions are those that after  $q$  periods of the internal frequency,  $\hat{\Phi}(t_0 + qT_b)$ , translates  $p_x$  and  $p_y$  lattice sites in the  $x$  and  $y$  direction of the square lattice, respectively, *i.e.*

$$\hat{\Phi}_{n,m}(t_0) = \hat{\Phi}_{n+p_x, m+p_y}(t_0 + qT_b) , \tag{19}$$

where again PBC are applied  $\Phi_{N_x+1,m} = \Phi_{1,m}$ ,  $\Phi_{0,m} = \Phi_{N_x,m}$ ,  $\Phi_{n, N_y+1} = \Phi_{n,1}$  and  $\Phi_{n,0} = \Phi_{n, N_y}$  (with  $N_x$  and  $N_y$  being the lattice size in the  $x$  and  $y$  direction respectively). Consequently, a  $(p_x, p_y, q)$ -resonant state will be a solution of the following set of equations

$$\begin{aligned}
F_{(p_x, p_y, q, \omega_b, \nu, C_1, C_2)}[\{\hat{\Phi}_{n,m}(t_0)\}] &= L_y^{p_y} L_x^{p_x} T_{(\omega_b, \nu, C_1, C_2)}^q[\{\hat{\Phi}_{n,m}(t_0)\}] = \\
&= \{\hat{\Phi}_{n,m}(t)\} ,
\end{aligned} \tag{20}$$

where the operators  $L_i$  are the lattice translation in the  $i$ -direction,

$$L_x[\{\Phi_{n,m}(t_0)\}] = \{\Phi_{n+1,m}(t_0)\}, \quad (21)$$

$$L_y[\{\Phi_{n,m}(t_0)\}] = \{\Phi_{n,m+1}(t_0)\}. \quad (22)$$

Besides,  $T_{(\omega_b, \nu, C_1, C_2)}$  is the time evolution operator given by equation (13) over one period  $T_b = 2\pi/\omega_b$ ,

$$T_{(\omega_b, \nu, C_1, C_2)}[\{\Phi_{n,m}(t_0)\}] = \{\Phi_{n,m}(t_0 + T_b)\}. \quad (23)$$

In order to illustrate the 2D time scales resonance we consider the plane wave solutions of equation (13):  $\Phi_{n,m}(t) = A \exp[i(k_x n + k_y m - \omega t)]$ . These solutions possess the following nonlinear dispersion relation

$$\omega(\vec{k}, A) = 2(C_1 \cos k_x + C_2 \cos k_y)(1 + \mu A^2) - 2\nu A^2. \quad (24)$$

Hence, we can obtain the subset of plane waves which are  $(p_x, p_y, q)$ -resonant with some time scale  $\tau$  (*i.e.* after a time  $q\tau$  they have translated  $p_x$  and  $p_y$  sites in the  $x$  and  $y$  direction, respectively). Each member of these subsets will be labelled by the pair  $\vec{k} = (k_x, k_y)$  and from the condition (20) it follows that the corresponding set of values of  $\vec{k}$  for each family will satisfy the relation

$$\omega(\vec{k}, A) = \frac{1}{q\tau} \left( \vec{p} \cdot \vec{k} - \frac{m}{2\pi} \right), \quad (25)$$

where  $m$  is an integer and  $\vec{p} = (p_x, p_y)$ . In figure 1 the corresponding values of  $\vec{k}$  are represented for two resonances of the type  $(p_x = 1, p_y = 0, q = 1)$  and  $(p_x = 1, p_y = 1, q = 1)$ .

The method used for solving equation (20) for each resonant 3-tuple  $(\omega_b, \vec{v}_b)$  is the same as in the 1D case, which is extensively described in [28]. The implicit function theorem assures that a fixed point solution of a map (20) given by  $\vec{\xi} = (p_x, p_y, q, \omega_b, \nu, C_1, C_2)$  can be obtained provided that (*i*) the Jacobian of the operator  $F_{\vec{\xi}}[\{\Phi_{n,m}(t_0)\}] - I$  is invertible and (*ii*) we know a fixed point of a map corresponding to an infinitesimally close set of parameters,  $\vec{\xi} - \delta\vec{\xi} = (p_x, p_y, q, \omega_b - \delta\omega_b, \nu - \delta\nu, C_1 - \delta C_1, C_2 - \delta C_2)$ . The first demand can be satisfied using a *singular value decomposition* (SVD) [43,44,45] of the Jacobian in order to obtain the pseudo-inverse operator. On the other hand, when the second condition is fulfilled convergence of the Newton-Raphson iterative scheme is guaranteed. For this, we start with a sufficiently good trial solution,  $\{\Phi_{n,m}^0(t_0)\}$  and solve the equation

$$\{\delta\Phi_{n,m}^0(t_0)\} = -DF_{\vec{\xi}}[\{\Phi_{n,m}^0(t_0)\}]^{-1} \cdot F_{\vec{\xi}}[\{\Phi_{n,m}^0(t_0)\}], \quad (26)$$

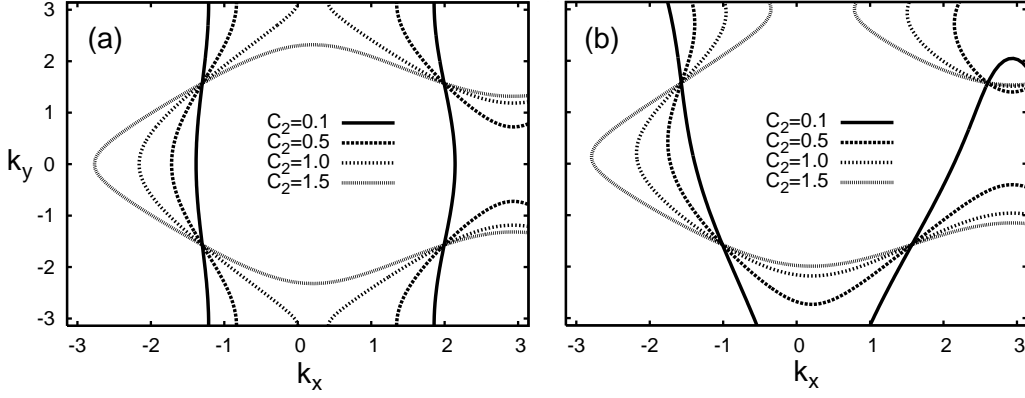


Fig. 1. Wave numbers,  $\vec{k} = (k_x, k_y)$ , of the (1,0,1) (a) and (1,1,1) (b) resonant plane waves for  $m = 0$  (see equation (25)). Different values of  $C_2$ , while  $C_1$  is fixed ( $C_1 = 1$ ), are shown. The reference time scale for the resonance is set to  $\tau = 2.4315$  ( $\omega = 2.584$ ).

in order to obtain  $\{\Phi_{n,m}^1(t_0)\} = \{\Phi_{n,m}^0(t_0)\} + \{\delta\Phi_{n,m}^0(t_0)\}$ . We iterate this calculations to the desired convergence, and then the solution  $\{\hat{\Phi}_{n,m}(t_0)\}$ , is obtained. In our numerics this is the case when

$$F_{\vec{\xi}}[\{\Phi_{n,m}^i(t_0)\}] < N \cdot 10^{-16}, \quad (27)$$

(where  $N$  is the total number of sites in the square lattice) is fulfilled. Once the solution is found we use it as the following trial solution,  $\{\Phi_{n,m}^0(t_0)\}$ , for solving the map (20) corresponding to the next set of parameters  $\vec{\xi}' = \vec{\xi} + \delta\vec{\xi}$ .

As an additional benefit, this method provides the linear stability of the computed solution. For this, we only have to compute the eigenvalues of the Jacobian of the operator around the solution  $DF_{\vec{\xi}}[\{\hat{\Phi}_{n,m}(t_0)\}]$ . In fact, this Jacobian is the extended Floquet matrix of the solution. Then, a solution is linearly stable if all the eigenvalues of the corresponding Floquet matrix are inside the unit circle. Moreover, the symplectic character of the dynamics (13) implies that all the eigenvalues appear in quadruplets  $(\lambda, \bar{\lambda}, 1/\lambda, 1/\bar{\lambda})$  and thus for a linearly stable solutions all the eigenvalues of its extended Floquet matrix lie on the unit circle.

There are two possible paths for developing the continuation method depending on the choice of the starting point of the continuation. One possibility is to start from the full anti-continuum limit,  $C_1 = C_2 = 0$ , where a pinned breather solution of frequency  $\omega_b$  is written as

$$\hat{\Phi}_{n,m}(t) = \delta_{n,n_0} \delta_{m,m_0} \sqrt{\frac{\omega_b}{2\nu}} \exp(i\omega_b t). \quad (28)$$

Starting from the above solution, we can perform the continuation increasing the parameters  $C_1$  and  $C_2$  as usual, and so obtain the whole family of  $(p_x = 0, p_y = 0, q = 1)$ -resonant discrete breathers. An alternative path starts from the one-dimensional limit,  $C_2 = 0$ . The choice of this second limit (which implies taking as the very initial trial solution of the continuation the whole set of 1D solutions described in section 2.1) is justified when seeking mobile solutions. As stated above, this limit offers the possibility of studying strongly anisotropic lattices as a controlled interpolating situation between one and two dimensions. On the other hand, employing this strategy we can only obtain those solutions which are  $(p_x = p, p_y = 0, q)$ -resonant, *i.e.* the two-dimensional continuation of those one-dimensional  $(p = p_x, q)$ -resonant discrete breathers. Hence, the solution from which we start is

$$\hat{\Phi}_{n,m}(t) = \delta_{m,m_0} \hat{\Phi}_n^{1D}(t) , \quad (29)$$

where  $\hat{\Phi}_n^{1D}(t)$  is the corresponding  $(p = p_x, q)$ -resonant one-dimensional solution.

In what follows we will employ both continuation paths when we study the case of pinned breathers (section 3), and we will show that the results obtained are the same when approaching the same limit (the standard two-dimensional DNLS).

### 3 Two-dimensional pinned discrete breathers

As we have discussed, we can choose two different starting points for the continuation of  $(0, 0, 1)$ -resonant fixed points (pinned breathers) of equation (20): *(i)* the full anti-continuum (AC) limit ( $C_1 = C_2 = 0$ ), or *(ii)* the (one-dimensional, 1D) limit of uncoupled chains ( $C_1 \neq 0, C_2 = 0$ ), where they can be obtained from continuation along increasing values of the parameter  $\nu$  from the 1D A-L lattice (1). As a test for our codes, we have checked that both paths arrive to the same solution. In fact, unique continuations can proceed along any path on the plane of parameters  $(C_2, \nu)$  that we have explored.

Early works [18,19,20] on the isotropic two-dimensional standard DNLS equation analyzed the so-called *quasi-collapse* instability of pinned discrete breathers, *i.e.* the condensation of all the energy into a few modes in discrete nonlinear systems, which corresponds to the onset of a singularity (wave collapse) [21] in multidimensional continuum models. Subsequent numerical works [22] extended these studies to the isotropic 2D Salerno lattice and addressed the question of how the instability is affected by the presence of impurity lattice sites.

As expected, our results further corroborate the existence of quasi-collapse instabilities in the anisotropic case: The phase diagram in parameter space  $(\omega_b, C_2, \nu)$  consists of two regions (stable and unstable) separated by the surface of transition. As we perform the continuation of breather solutions across the parameter space we scan the Floquet stability of the computed solution. In figure 2 we present the two stability transition curves in the plane  $(\omega_b, C_2, \nu = 1)$ , *i.e.* the function  $C_2^{th}(\omega_b)$ , corresponding to the two different continuation starts. The continuation from the AC limit is made through the path  $C_1 = C_2$  and the one from the 1D limit is made at  $C_1 = 1$ . The convergence of the two paths at  $C_2 = 1$  is clearly seen.

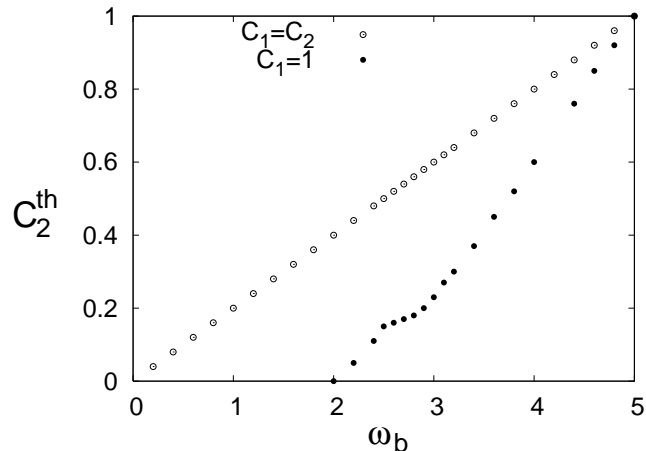


Fig. 2. Evolution of the threshold value of the coupling parameter,  $C_2^{th}$ , as a function of the frequency,  $\omega_b$ , for two different continuations starts. The values of  $C_2^{th}$  limit the region where pinned discrete breathers are linearly stable (unstable for  $C_2 > C_2^{th}$ ). The instability yields a hyper-localized state (quasi-collapse). The continuation from the fully uncoupled limit ( $C_1 = C_2 = 0$ ) (filled circles) is performed using the path  $C_1 = C_2$ . For the continuation (bold circles) from the 1-dimensional limit ( $C_1 = 1, C_2 = 0$ ) the coupling in the new direction  $C_2$  is progressively increased.

The criterion for stability of the pinned discrete breather solution derived in [19,20],

$$\left( \frac{\partial \mathcal{N}}{\partial \omega_b} \right)_{C_2, \nu} > 0, \quad (30)$$

is of a very general character and our numerics illustrate it clearly. On the other hand, the Floquet stability analysis detects the dimensionality (and a basis in tangent space) of the unstable linear manifold associated with the quasi-collapse instability that these exact discrete breathers experience for some parameter values. We have computed numerically, for a fine grid of  $\omega_b$  values and a coarser grid of  $C_2$  and  $\nu$ , the function  $\mathcal{N}(\omega_b, C_2, \nu)$ , from which

we show some sectors in figures 3 and 4.

In figure 3 we show the numerically computed norm (16) as a function of the breather frequency  $\mathcal{N}(\omega_b)$ , for three different values of the transversal coupling  $C_2$ , and a fixed value of  $\nu = 1$  (anisotropic DNLS limit). We observe the existence of a minimum value,  $\min \mathcal{N}(\omega_b) = \mathcal{N}^{th} \neq 0$ , which is thus seen as an *excitation threshold* for the creation of these solutions. The position of the minimum  $\omega_b^{th}(C_2)$ , which *naturally* increases with  $C_2$ , separates the stable and unstable branches of pinned breathers. Breathers corresponding to values of  $\omega_b$  where  $\mathcal{N}(\omega_b)$  has a negative slope are unstable: This is shown in the insets, where the Floquet spectra of two representative examples of pinned discrete Schrödinger breathers are plotted in the complex plane. Note that the high accuracy of the numerical solution allows an unprecedented detailed Floquet analysis of the instability, paving the way to rigorous analytical characterizations of the quasi-collapse unstable manifold. This is a one-dimensional manifold, as our numerical results unambiguously confirm. Then, in the regime of small time scales, the unstable manifold is fully characterized by a single Floquet eigenvector.

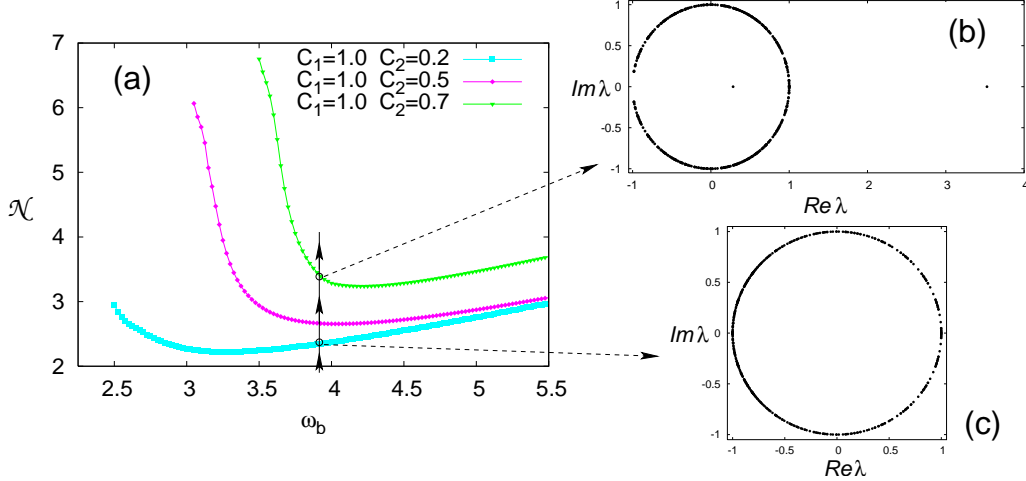


Fig. 3. **(a)** Plot of the Norm,  $\mathcal{N}$ , of the computed solutions as a function of their frequency  $\omega_b$  for different values of the coupling parameters. The continuations have been made starting from the 1-dimensional limit ( $C_1 = 1$ ). For the regions where  $\partial \mathcal{N} / \partial \omega_b$  is positive (negative) the continued solutions are stable (unstable). We can monitor the change of the linear stability of a solution of a given frequency during its continuation in  $C_2$  looking at the Floquet spectra. Figures **(b)** and **(c)** show the Floquet spectra of a discrete breather of frequency  $\omega_b = 3.93$  at  $C_1 = 1, C_2 = 0.7$  (where  $\partial \mathcal{N} / \partial \omega_b < 0$ ) and at  $C_1 = 1, C_2 = 0.2$  (where  $\partial \mathcal{N} / \partial \omega_b > 0$ ), respectively.

Figure 4 shows the (surface) function  $\mathcal{N}(\omega_b, \nu)$  for the volume sector of constant  $C_2 (= 0.5)$ . Most noticeably, the critical (threshold) line of bifurcation points ( $\frac{\partial \mathcal{N}}{\partial \omega_b} = 0$ ), as seen in the inset, does not define a monotone function  $\omega_b^{th}(\nu)$ . In fact, in the whole interval of  $0 \leq \nu \leq 1$  values, the range of values of

$\omega_b^{th}$  is quite short, indicating the insensitivity of the gross features of the quasi-collapse transition to the value of  $\nu$ . However, considering finer details, one sees that the threshold curve  $\omega_b^{th}(\nu)$  smoothly reaches its slightly larger values around midway between the DNLS and the A-L limits. In other words, intermediate values of the interpolating (Salerno) parameter  $\nu$  somewhat favour the enhancement of the quasi-collapse unstable region. These conclusions are in contrast with the stated conclusion (for isotropic lattices) in [22] that the Ablowitz-Ladik term increases the stability regime.

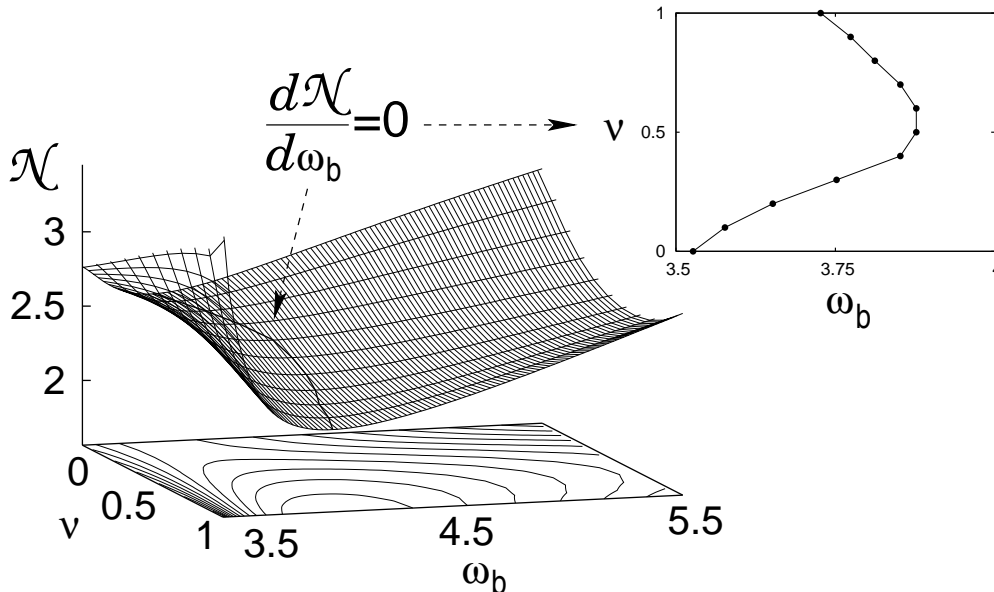


Fig. 4. Surface  $\mathcal{N}(\omega_b, \nu)$  for the case  $C_2 = 0.5$ . The inset shows the curve  $\nu(\omega_b)$  corresponding to  $\partial\mathcal{N}/\partial\omega_b = 0$ . This curve gives the transition points where the discrete breather changes its stability character.

When instability is allowed to develop beyond the fixed point tangent space into the nonlinear realm of perturbations, the trajectory obtained by direct integration of the equations of motion invariably ends after a transient (of time scale given by the real Floquet exponent larger than 1) in a localized solution with complex dynamics, the *pulson states*. These states were characterized in [3] in the following terms "... where the peak intensity  $|\Phi_{m,n}|^2$  oscillates between the central site and its four nearest neighbours... it is not known whether these pulson states represent true quasiperiodic solutions to the DNLS equation". What makes these trajectories on the unstable nonlinear quasi-collapse manifold of much practical relevance and interest is their ubiquity: They appear as persistent localized states in the hamiltonian dynamical evolution from a wide variety of initial conditions. Their description requires at least two frequencies, namely the internal (genuine breather-like

frequency) and the frequency of the oscillations of the *breather width* around a mean width value, which turns out to be less than the width of the unstable exact discrete breather. Second and outer shells of neighbours (in both lattice axes) also participate in the width oscillations.

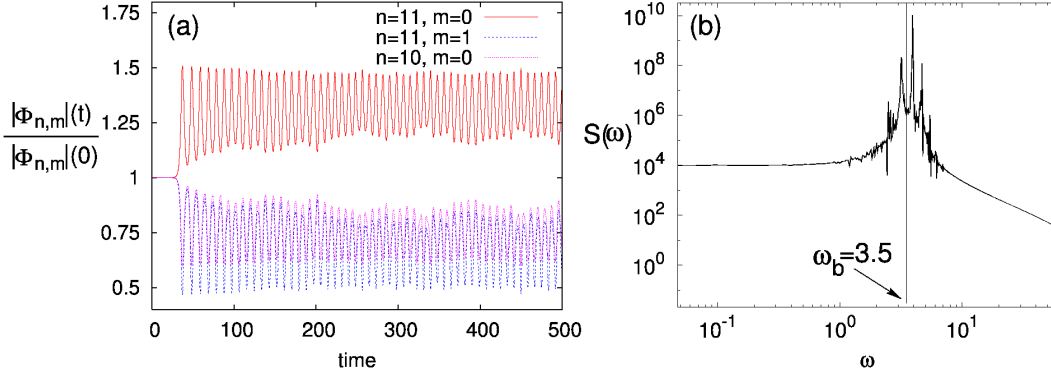


Fig. 5. (a) Time evolution of the amplitude  $|\Phi_{n,m}|$  for the localization center ( $n = 11$ ,  $m = 0$ ) and two adjacent sites ( $n = 10$ ,  $m = 0$ ) and ( $n = 11$ ,  $m = 1$ ). Each amplitude is normalized to its initial value, so that it can be seen how the quasi-collapse instability is developed. The parameters of equation (13) are  $C_1 = 1$ ,  $C_2 = 0.5$ ,  $\nu = 1.0$  ( $\mu = 0$ ) and the frequency of the pinned breather is  $\omega_b = 3.50$ . When the instability is fully developed, we analyse the final state by means of the Power Spectrum  $S(\omega)$  of the time evolution of  $\Re[\Phi_{10,0}(t)]$  (the real part of localization center). As can be observed in (b) the internal frequency of the breather (highest peak in the spectrum) shifts to a higher value ( $\omega_b^* = 4.03$ ) and the other peaks are located at the frequencies of the harmonics resulting from the combination of the internal frequency with the frequency ( $\omega_{qc} = 0.78$ ) associated with the amplitude  $|\Phi_{n,m}|$  oscillations shown in (a).

Though a more detailed characterization of the pulson states will be presented elsewhere, it is illustrative to consider (figure 5) the power spectrum of the field at the central site of a typical trajectory on the unstable nonlinear manifold of a quasi-collapsing pinned discrete breather. This shows peaks at the combinations  $\omega_b^* + j\omega_{qc}$  ( $j = 0, \pm 1, \pm 2, \dots$ ), where  $\omega_{qc}$  is the frequency of the width oscillations characterizing the pulson state, while  $\omega_b^* > \omega_b$  is a frequency higher than the (initial condition) fixed point frequency  $\omega_b$ . The new frequency  $\omega_b^*$  turns out to be very close to the breather frequency of the same (initial) norm on the stable branch. In other words, the instability drives a shift of breathing frequency towards the stable branch, while the excess energy is transferred to the oscillatory motion of the observable width. This behavior seems to be the essence of the physical characterization of the nonlinear quasi-collapse manifold dynamics.

The numerical observation of a two-frequency power spectrum for a typical pulson state points towards an eventual positive answer to the question (on true quasiperiodicity) arised in [3], though, for more details we have to refer to

the PhD dissertation [46]. This point serves to illustrate how the high accuracy of the fixed point numerical solution provides detailed clues on many still unsolved (from a mathematical and physical point of view) questions on two-dimensional Schrödinger localization, which are of prospective experimental interest in nonlinear (photonic, Josephson, ...) physics technologies.

#### 4 Breathers moving along the strong coupling direction.

Early and current attempts to explore straightaway discrete breather mobility in isotropic 2D Schrödinger lattices seem to agree [47] that "kicking" procedures meet huge difficulties in delivering good mobile solutions, contrary to the numerical experiences in 1D lattices. We note here that the formal basis for those methods [48] takes advantage of the Floquet spectra analysis of exact pinned breathers, where the so-called *depinning* (symmetry-breaking) mode is identified. This allows, *provided Peierls-Nabarro barriers are small enough*, to obtain nice numerical 1D mobile discrete breathers, by computing trajectories from perturbations of the exact pinned breather along the tangent space direction specified by the depinning eigenvector. The presence of symmetry-breaking instabilities leading to exchange of stability between one-site and two-site centered pinned breathers [45,49] and the associated lowering of the Peierls-Nabarro barriers to breather displacements, hugely facilitating the success of these procedures when applied to (both hamiltonian and dissipative) one-dimensional lattices. [50,51,52]

In contrast, our "anisotropic lattice" continuation approach takes advantage of the availability of exact 1D mobile solutions by monitoring the parameter  $C_2$  of transversal coupling, and then does not rely on how easily one promotes clean mobility from pinned localization. In this way we obtain accurate numerical  $(p_x, p_y = 0, q)$  fixed points, that is Schrödinger discrete breathers moving along the strong coupling direction. In a forthcoming paper we will address the (much more difficult) question for arbitrary direction of motion.

##### 4.1 Structure and stability of $(1,0,1)$ fixed points.

In figure 6 we visualize the instantaneous real and imaginary components of the 2D discrete field profile of a typical  $(1,0,1)$  Schrödinger breather. Its structure can be seen as the natural extension to two-dimensional lattices of the structure of mobile Schrödinger breathers analyzed in [27,28]. The numerical solution is spatially asymptotic to a *finely tuned* small-amplitude extended (de-localized) radiation state  $\Phi_{m,n}^{\text{bckg}}(t)$  when  $m, n \rightarrow \infty$ . The fixed point solution

can be thus decomposed as

$$\Phi_{m,n}(t) = \Phi_{m,n}^{\text{core}}(t) + \Phi_{m,n}^{\text{bckg}}(t), \quad (31)$$

which defines  $\Phi_{m,n}^{\text{core}}(t)$ , the spatially *localized* component of the solution. It turns out that the spatially *delocalized* component is a highly localized state in the (continuum, in the thermodynamic limit)  $k$ -space of wavevectors. More precisely,  $\Phi_{m,n}^{\text{bckg}}(t)$  is a finite linear combination of  $(1,0,1)$ -resonant nonlinear (*i.e.* amplitude-dependent frequency  $\omega$ ) 2D planewaves. It can be said that, as might be expected, 1D Schrödinger breather mobility smoothly persists when (strong  $C_1$ -coupling) 1D chains are coupled transversally. Importantly, the numerical continuation for increasing values of the transversal coupling  $C_2$  proceeds far from the weak coupling regime into where the genuine two-dimensional effects start to be manifest, as we will see below.

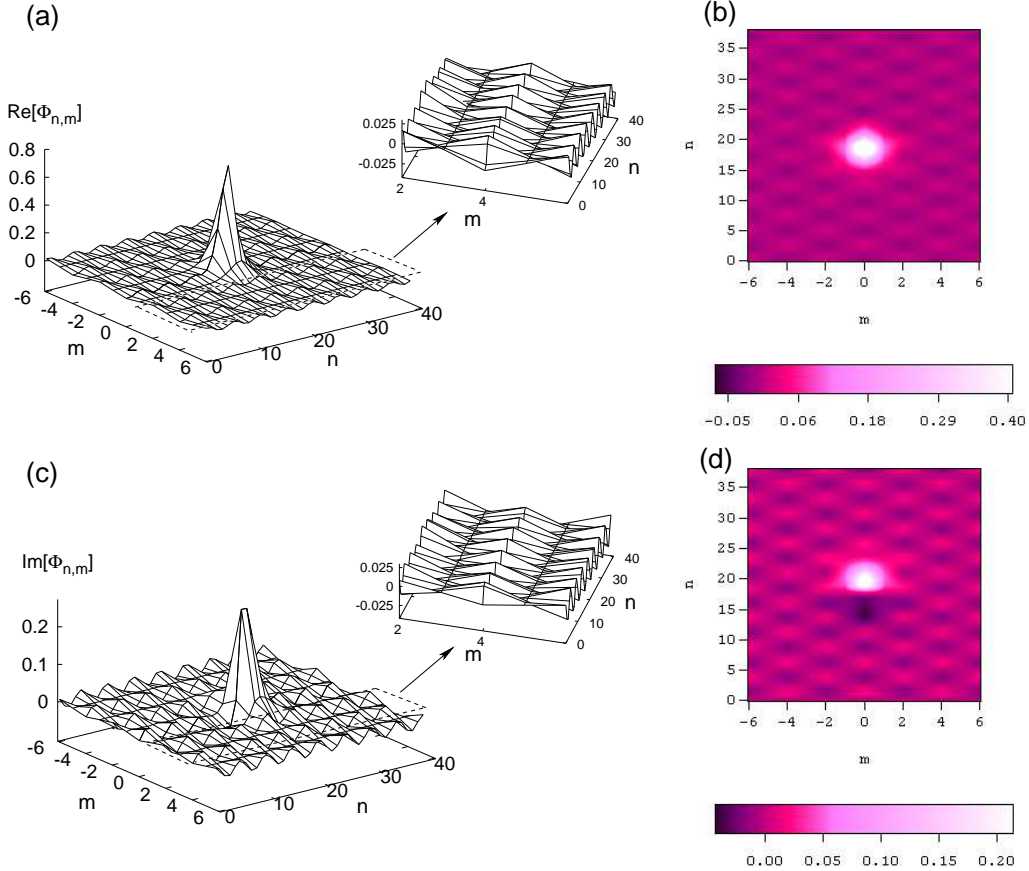


Fig. 6. Real, (a) and (b), and imaginary, (c) and (d), of a mobile  $(1,0,1)$ -discrete breather of frequency  $\omega_b = 2.712$ . The parameters of equation (13) are  $C_1 = 1$ ,  $C_2 = 0.14$  and  $\nu = 0.95$  ( $\mu = 0.05$ ). The insets in (a) and (c) show the background far from the moving core. It can be observed that the wavenumbers in the transversal direction are  $k_y = \pm\pi/2$ . (b) and (d) show the contour plot for both real and imaginary parts.

Most noticeable, the SVD-regularized Newton procedure invariably selects the values  $k_y = \pm\pi/2$  for all values of  $C_2$  and  $\nu$ , and thus the values of  $k_x$  for the 2D resonant planewave are independent of  $C_2$  (so it remains equal to the  $k$  values of the 1D  $(1, 1)$  fixed point for the uncoupled chain). The appearance of an extended background modulation in the transversal direction of  $k_y = \pm\pi/2$  appears naturally as the *best* choice to take advantage of approximately 1D breather propagation along strong coupling direction, for it keeps the value of  $k_x$  favoured by the strong coupling  $C_1$  value: Any other value of  $k_y$  would entail a different  $k_x$  value. Note however that this provides only a *plausibility argument* for the interpretation of the numerical observation ( $k_y = \pm\pi/2$ ).

The high accuracy of the computed solutions allows a detailed analysis of many issues concerning 2D Schrödinger breather exact mobility along the strong coupling direction. We leave aside in this paper many of them, and focus here on how the existence of quasi-collapse instabilities of pinned Schrödinger breathers, for increasing  $C_2$ -coupling values, influences the stability properties of moving  $(1, 0, 1)$  breathers. In other words, we search here for genuine 2D effects on these "strong-coupling -direction" (quasi-1D) moving breathers.

We have performed an exhaustive exploration of two sectors of the parameter space  $(C_2, \omega_b, \nu)$ , corresponding to the breather frequency values  $\omega_b = 2.5843$ , and  $\omega_b = 2.712$ , by computing the continued  $(1, 0, 1)$  fixed point. These values of  $\omega_b$  were chosen low enough to allow the analysis of pinned breather quasi-collapse effects on mobility, which occurs at relatively low values of  $C_2^{th}(\nu)$  for these values of  $\omega$ .

The Floquet analysis of the computed solutions provides the stability diagrams represented in figures 7. Both show no qualitative differences: There are two regions in the  $(C_2, \nu)$  plane where the  $(1, 0, 1)$  mobile breather is linearly unstable. The figures are not "schematic": Every point of the plane in a fine grid of values of  $C_2$  and  $\nu$  has been analyzed, *i.e.* the Floquet spectrum of the computed  $(1, 0, 1)$  fixed point is scrutinized, as shown in figures 7.b and 7.d, where the modulus of the Floquet eigenvalues is shown as a function of either  $\nu$  (figure 7.b) or  $C_2$  (figure 7.d).

The first unstable region appears at low values of  $C_2$  and intermediate to high values of the Salerno parameter  $\nu$ , *i.e.* it does not occur close to the A-L limit. This unstable region is also bounded above in the direction of  $C_2$ : The variation of the modulus of the unstable Floquet eigenvalue versus the transversal coupling parameter  $C_2$  shows that the mobile breather becomes stable again at larger values of  $C_2$ , before the second instability at even higher coupling takes place. An important observation is that the pinned discrete breather of the same frequency is *linearly stable* at the points in this unstable region for  $(1,0,1)$  mobile breathers. Thus this instability cannot be ascribed to pinned quasi-collapse effects.

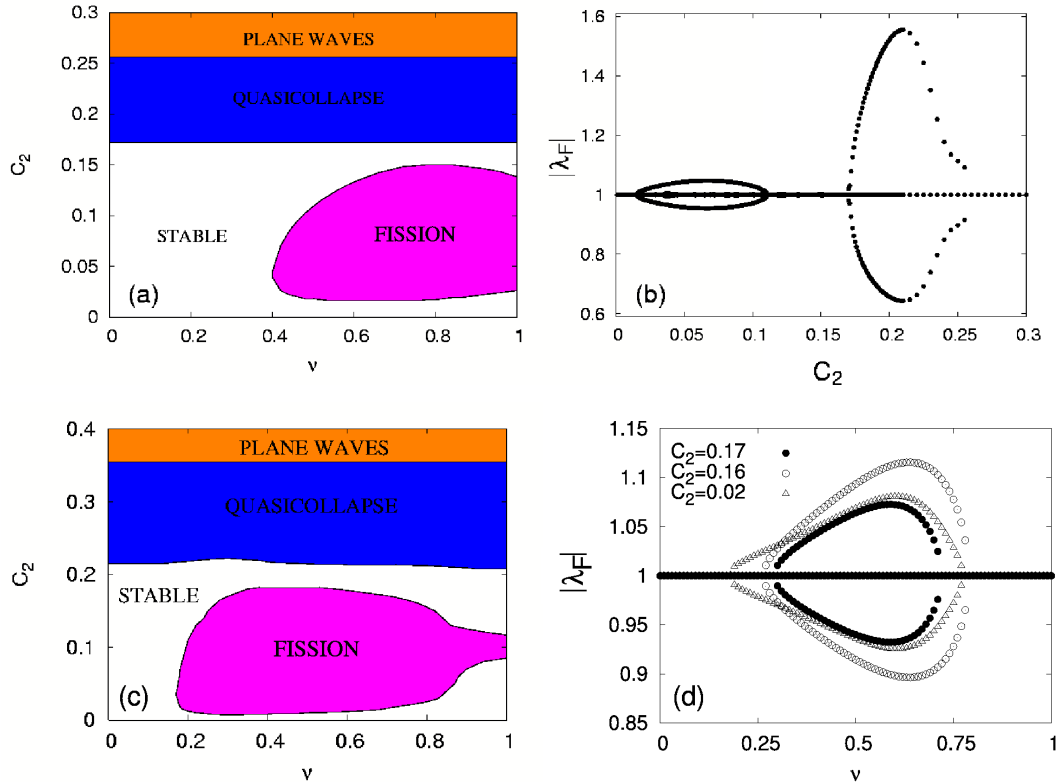


Fig. 7. Stability diagram and evolution of the modulus of the Floquet eigenvalues for two  $(1, 0, 1)$ -discrete breather of frequencies  $\omega_b = 2.584$  (a) and (b), and  $\omega_b = 2.712$  (c) and (d). The stability diagram (a) and (c) show two regions where the mobile DB becomes unstable. For low values of the coupling  $C_2$  there is a subset of values of  $\nu$  where the breather suffers from fission (see text and figures (8.a) and (8.b)). On the other hand for higher values of  $C_2$  there is a second region (quasi independent of  $\nu$ ) where the unstable breather yields a travelling quasi-collapsing state (see text and figures (8.c) and (8.d)). The evolution of the modulus of the Floquet eigenvalues along different paths  $\nu = 0.50$  (b) and  $C_2 = 0.17, 0.16, 0.02$  (c) is shown.

The second transition occurs for values of  $C_2$  close to, but slightly higher than, the values  $C_2^{th}$  of the quasi-collapse of the pinned breather of the same frequency. We had already seen in the previous section that the quasi-collapse transition  $C_2^{th}(\nu)$  is only very weakly dependent on the value of  $\nu$ , and note that the same is true for this mobile breather bifurcation. These results suggest that this second transition is related to quasi-collapsing phenomena. Significantly, the stability of the  $(1, 0, 1)$  mobile breather persists for a small interval of coupling values above the pinned breather quasi-collapse. This should be regarded as natural, for the mobile breather is a different solution. Note in figure 7.b that the modulus of the unstable Floquet eigenvalue, in the interior of the unstable region, reaches much higher values than those typical for the first type of instability, and decreases for larger values of  $C_2$ , before the breather solution ceases to exist and only plane wave solutions are obtained by our numerical method. Note that this behaviour of the unstable Floquet

eigenvalue also fits well to the main features of the pinned quasi-collapse instability strength, as described by the slope  $\partial\mathcal{N}/\partial\omega_b$ . From now on we will refer to this instability of mobile breathers as the quasi-collapse instability.

In the next subsection we characterize both generic types of instability, by looking at the details of the unstable manifold associated with each type. As we will see, pulson states turn out to play a role in the description of typical trajectories on the unstable nonlinear manifolds.

#### 4.2 *Unstable manifold behaviour and ubiquity of pulson states.*

First, we analyze the quasi-collapse instability of  $(1, 0, 1)$  mobile breathers. The unstable linear subspace in the tangent space of the fixed point is one-dimensional. The typical instantaneous profile of the (modulus) unstable Floquet eigenvector driving the instability is shown in figure 8.d. It is an exponentially localized 2D profile which decays asymptotically to zero as  $m, n \rightarrow \infty$ , *i.e.* it does not excite radiation. These characteristics are shared by the quasi-collapse unstable eigenvector of the pinned breathers, which further reinforce the previous considerations leading us to consider this instability as the mobile counterpart of the pinned quasi-collapse transition.

In figure 8.c we have visualized the time evolution of the field modulus contour plot for a typical trajectory on the unstable manifold. This is obtained by direct numerical integration of the equations of motion, from an initial condition in which a small perturbation along the quasi-collapse eigenvector has been added to the unstable fixed point solution. One sees that the breather translational motion slows down, and the energy is transferred to width oscillations. These oscillations turn out to be more irregular, see figure 9, than those observed in section 3 when we inspected typical trajectories on the unstable nonlinear manifold of pinned breathers.

The difference in the character of the width oscillations in both (pinned and mobile) cases may be ascribed to the presence of an extended background component in the mobile breather solution, which naturally enters into the energy transfer taking place during temporal evolution. The slowing down of the translational motion continues and eventually the breather pins into a convulsive pulson state surrounded by the remaining radiation.

Now we pay attention to the “low  $C_2$ ” instability of  $(1, 0, 1)$  mobile breathers. The modulus profile of the unstable Floquet eigenvector that drives this instability is M-shaped (bimodal), as shown in figure 8.b, and is asymptotic to an extended planewave-like profile as  $m, n \rightarrow \infty$ , *i.e.* it is not a purely localized perturbation. It is indeed rather different from the quasi-collapse unstable eigenvector analyzed above, which is consistent with the fact that the pinned

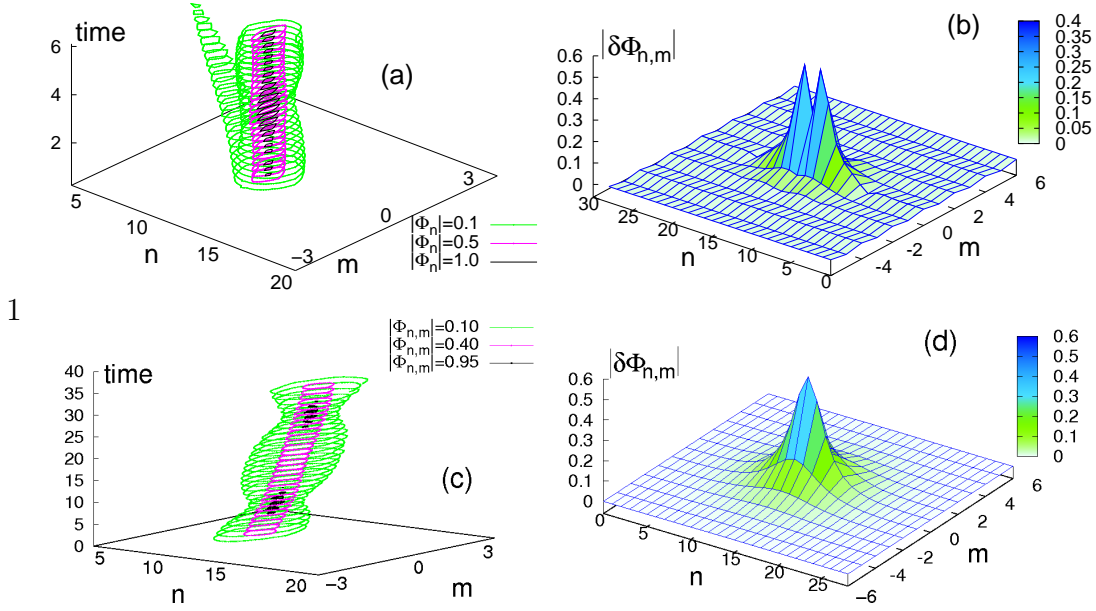


Fig. 8. Time evolution of two unstable solutions, **(a)** and **(c)**, of frequency  $\omega_{ab} = 2.584$  and the associated unstable Floquet eigenvector, **(b)** and **(d)** respectively. Figures **(a)** and **(c)** show the time evolution of the contour lines corresponding to three different values of  $|\Phi_{n,m}|$ , in order to visualize the 4-dimensional functions  $|\Phi_{n,m}|(t)$ . Figures **(a)** and **(b)** shows the fission of the breather solution when perturbed along the unstable “M-shaped” Floquet eigenvector plotted in **(b)**. It can be seen how a low amplitude pulse emerges and the mobile breather becomes pinned. After this transient this low amplitude pulse decays into radiation. The parameter of equation (13) are  $C_1 = 1$ ,  $C_2 = 0.08$  and  $\nu = 0.5$  ( $\mu = 0.5$ ). In the case of figures **(c)** and **(d)** the parameters are the same except for  $C_2 = 0.19$ . In this case the solution is in the “quasi-collapse” unstable region shown in figure (7.a). The final state when perturbed along the unstable eigenvector **(d)** is a travelling breather whose amplitude oscillates in the same fashion as that of the pinned quasi-collapsing breathers, *i.e.* the localization center oscillates out of phase with respect to all the other sites on the lattice.

breather of the same frequency is linearly stable in this region of parameter space. As argued above, this instability is not related to quasi-collapse phenomena, and it does not appear in the region of small values of the Salerno parameter  $\nu$ , close to the A-L limit.

A typical trajectory on the unstable manifold associated with this instability is shown in figure 8.a, where we have plotted the time evolution of the field modulus contour plot. We can see there that the mobile breather pins quickly while a small pulse moving backwards is ejected, which spreads and finally mixes with the remaining delocalized background. However some energy is transferred to width oscillations of the pinned breather so that also in this case we observe the formation of pulson states surrounded by the remaining radiation. As the main difference of this behaviour, with respect to the evo-

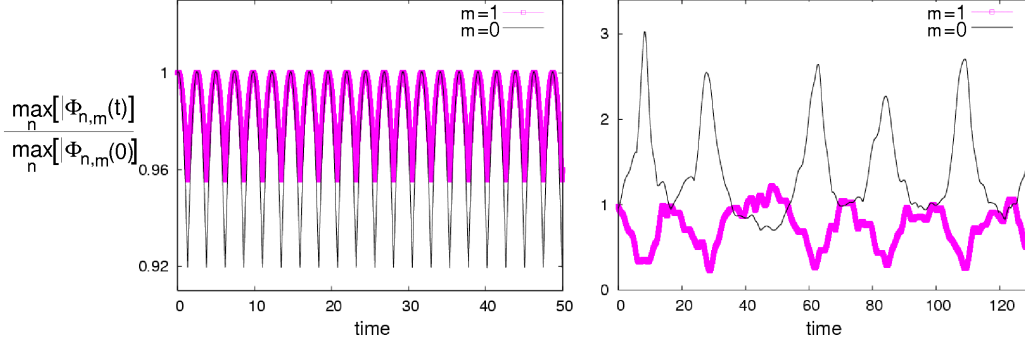


Fig. 9. Time evolution of the maximum value of the modulus  $|\Phi_{n,m}|(t)$  along the central ( $m = 0$ ) chain and the adjacent ( $m = 1$ ) one for a mobile  $(1, 0, 1)$  breather with frequency  $\omega_b = 2.584$ . This magnitude is normalized to the initial value  $|\Phi_{n,m}|(t_0)$ . Figure **(a)** shows this evolution for an stable situation ( $C_2 = 0.15$ ,  $\nu = 0.5$ ). It can be observed how the localization center ( $m = 0$ ) and its neighbour in the transversal direction ( $m = 1$ ) follows two in-phase periodic trajectories in their modulus due to the Peierls-Nabarro barrier surpassed during the motion. In contrast, figure **(b)**, shows the case when the breather is unstable ( $C_2 = 0.19$ ,  $\nu = 0.5$ ). Here the quasi-collapse dynamics is manifested while the localization center moves across the lattice. As can be observed, the oscillations of the two amplitudes are out of phase and the amplitudes of these oscillations are one order of magnitude higher than those of figure **(a)**.

lution observed on the quasi-collapse unstable manifold, is the ejection of the small moving pulse, we refer to this instability as *fission*.

By increasing the strength of the initial perturbation along the direction of the unstable eigenvector, one observes that the size of the ejected pulse increases. This observation is consistent with the results reported in [22], where the evolution of initial moving gaussian pulses in isotropic 2D Schrödinger lattices was studied. These numerical experiences lead the authors to conclude that "the characteristic feature of the discrete quasi-collapse of a moving pulse is the splitting of the initially moving broad pulse into a track of the standing narrow structures ..." (sic). However, we see from our study of the stability of exact moving discrete breathers that the fission and the quasi-collapse instabilities have different origins and they appear in different regions of parameter space. On the other hand, the ubiquitous phenomenon of width oscillations of pinned localized structures (pulsion states) cannot be ascribed to quasi-collapse. They also appear as the preferred way to allocate excess of (localization) energy in regions of parameter space far from the quasi-collapse unstable region.

## 5 Conclusions and Prospective Remarks

We have studied here the dynamics of exact numerical discrete breathers, both pinned and mobile, in two-dimensional anisotropic nonlinear Schrödinger lattices. These solutions are computed using a SVD-regularized Newton method by continuation from a set of uncoupled 1D chains into increasing non-zero values of the coupling in the transversal direction.

We have performed an extensive exploration in the parameter space  $(\omega_b, C_2, \nu)$  of breather frequency, transversal coupling and Salerno parameter, by computing the Floquet spectra of the numerical solutions. We have also computed the breather norm  $\mathcal{N}(\omega_b, C_2, \nu)$  and further corroborate the general validity of the criterion found in [20], namely that the partial derivative  $\partial\mathcal{N}/\partial\omega_b$  is positive for stable pinned breathers. Furthermore, we have analyzed the dynamics on the quasi-collapse unstable manifold, where the unstable breather experiences a shift in frequency towards the (higher) value of the stable breather with the same norm. The excess of energy is coherently transferred to oscillations of the breather width, so that the resulting pulson state is characterized by two frequencies.

We have studied discrete breathers moving along the strong coupling direction. These solutions are composed of an exponentially localized core on top of an extended background which is itself the finite sum of a finite set of nonlinear 2D plane waves. The time scales associated with these plane waves are resonant with the core internal frequency as happens in the 1D case. In particular, the background chooses a finite set of plane waves from a continuous family of resonant solutions. The Floquet analysis of these mobile discrete breathers reveals the existence of two distinct types of instability. One is the counterpart, for mobile breathers, of the quasi-collapse experienced by pinned breathers. The other instability occurs in a region of parameter space where pinned breathers are linearly stable. The analysis of the dynamics on the unstable manifold show that the excess of energy is partly transferred to a small moving pulse, ejected from the center of localization, which justifies the designation of a fission instability. However, part of the energy excess is also transferred to width oscillations. The appearance of pulson states far from the quasi-collapse regime indicates that the tendency to allocate energy in the form of width oscillations is a general 2D feature, not exclusively associated to quasi-collapse instabilities.

In a future work we will focus on mobility of 2D discrete breathers in an arbitrary lattice direction. The results obtained here shed light about how this mobility can be obtained. In fact, our experiences show that mobility of pinned breathers can be induced based on the existence of the extended background in the numerically exact mobile solution. On the other hand, the results ob-

tained here and the aforementioned future work may help to design and better understand recent numerical experiments reported in [53], concerning the interaction between high amplitude pinned breathers and mobile ones. These experiments provides a possible way for routing and blocking mobile discrete breathers via the interaction with the high amplitude pinned ones, resulting in a plausible implementation of logical functions.

## 6 Acknowledgments

The authors acknowledge F. Falo, Yu. Kivshar, R.S. Mackay and M. Peyrard for sharing thoughts, and pointing out some important references to us. JG-G and LMF are grateful to M. Johansson and B. Malomed for discussions on some issues regarding the "travelling wave" (orthodox) perspective on discrete breathers. Financial support came from MCyT (Project No. BFM2002 00113), DGA and BIFI. JG-G acknowledges financial support from the MECyD through a FPU grant. Work at Los Alamos performed under the auspices of the US DoE.

## References

- [1] A.C. Scott, *Nonlinear Science: Emergence and Dynamics Structures* (Oxford University Press, Oxford, 1999).
- [2] R. S. Mackay and S. Aubry, *Nonlinearity* **7**, 1623 (1994).
- [3] J. C. Eilbeck and M. Johansson, in *Proceedings of Localization and Energy Transfer in Nonlinear Systems*, edited by L. Vázquez, R. S. MacKay, and M. P. Zorzano (World Scientific, Singapore, 2003),p.44.
- [4] P.G. Kevrekidis, K.Ø. Rasmussen and A.R. Bishop, *Int. J. Mod. Phys. B* **15**, 2833 (2001).
- [5] D.N. Christodoulides and R.I. Joseph, *Opt. Lett.* **13**, 794 (1988).
- [6] A.B. Aceves *et al*, *Opt. Lett.* **19**, 332 (1994).
- [7] A.B. Aceves *et al*, *Phys. Rev. E* **53**, 1172 (1996).
- [8] H. Eiseberg *et al*, *Phys. Rev. Lett.* **81**, 3383 (1998)
- [9] R. Morandotti *et al*, *Phys. Rev. Lett.* **83**, 2726 (1999)
- [10] P.G. Kevrekidis, K.Ø. Rasmussen and A.R. Bishop, *Phys. Rev. E* **61**, 2006 (2000).

- [11] P.G. Kevrekidis, K.Ø. Rasmussen and A.R. Bishop, Phys. Rev. E **61**, 4652 (2000).
- [12] B.A. Malomed and P.G. Kevrekidis, Phys. Rev. E **64**, 026601 (2001).
- [13] S. Flach, K. Kladko and R.S. MacKay, Phys. Rev. Lett. **78**, 1207 (1997).
- [14] M.I. Weinstein, Nonlinearity **12**, 673 (1999).
- [15] M. Kastner, Phys. Rev. Lett. **92**, 104301 (2004).
- [16] M. Kastner, Nonlinearity **17**, 1923 (2004).
- [17] G. Kalosakas, K. Ø. Rasmussen and A.R. Bishop, Phys. Rev. Lett. **89**, 030402 (2002).
- [18] V.K. Mezentsev, S.L. Musher, I.V. Ryzhenkova and S.K. Turitsyn, JETP Lett. **60**, 829 (1994).
- [19] E.W. Laedke, K.H. Spatschek and S.K. Turitsyn, Phys. Rev. Lett. **73**, 1055 (1994).
- [20] E.W. Laedke *et al*, JETP Lett. **62**, 677 (1995).
- [21] J.J. Rasmussen and K. Rypdal, Phys. Scr. **33**, 481 (1986).
- [22] P.L. Christiansen *et al*, Phys. Rev. B **54**, 900 (1996).
- [23] P.L. Christiansen *et al*, Phys. Scr. **67**, 160 (1996).
- [24] N.K. Efremidis *et al*, Phys. Rev. E **66**, 046602 (2002).
- [25] J. Fleisher *et al*, Phys. Rev. Lett. **90**, 023902 (2003).
- [26] J. Fleisher *et al*, Nature **422**, 147 (2003).
- [27] J. Gómez-Gardeñes, F. Falo and L.M. Floría, Phys. Lett. A **332**, 213 (2004).
- [28] J. Gómez-Gardeñes, L.M. Floría, M. Peyrard and A.R. Bishop, Chaos **14**, 1130 (2004).
- [29] M.J. Ablowitz, Z.H. Musslimani and G. Biondini, Phys. Rev. E **65**, 026602 (2002).
- [30] Y. Sire and G. James, Physica D **204**, 15 (2005).
- [31] G. James and Y. Sire, Commun. Math. Phys. **257**, 51 (2005).
- [32] J. L. Marín and S. Aubry, Nonlinearity **9**, 1501 (1996).
- [33] J.L. Marín. PhD dissertation. University of Zaragoza (1997).
- [34] S. Aubry and T. Cretegny, Physica D **119**, 34 (1998).
- [35] S. Flach and K. Kladko, Physica D **127**, 61 (1999).
- [36] B. Sánchez-Brey and M. Johansson, Phys. Rev. E **71**, 036627 (2005).

- [37] M.J. Ablowitz and J.F. Ladik, *Stud. Appl. Math.* **55**, 213 (1976); *J. Math. Phys.* **17**, 1011 (1976).
- [38] M. Salerno, *Phys. Rev. A* **46**, 6856 (1992).
- [39] H. Feddersen, in M. Remoissenet and M. Peyrard, eds., *Nonlinear coherent structures in physics and biology*, Lecture Notes in Physics **393**, 159 (Springer-Verlag, Berlin, 1991).
- [40] S. Aubry in *Structures et Instabilités*, C. Godréche ed. (Les Ulis, France: Editions de Physique, 1985).
- [41] D. Cheskis *et al*, *HAIT J. Sci. Eng.* **1**, 363 (2004).
- [42] T. Peschel and F. Lederer, Proceedings of the Conference on Nonlinear Coherent Structures in Physics and Biology, D.B. Duncan and J.C. Eilbeck eds., published on WWW: <http://www.ma.hw.ac.uk/solitons/procs/>
- [43] G. Strang, *Linear Algebra*, 2nd ed. (Academic, New York, 1980).
- [44] T. Cretegny and S. Aubry, *Phys. Rev. B* **55**, R11929 (1997).
- [45] Th. Cretegny. PhD dissertation. ENS Lyon (1998).
- [46] J. Gómez-Gardeñes, **PhD dissertation**. (In preparation) University of Zaragoza (2006).
- [47] J. Cuevas, private communication (2005).
- [48] D. Chen, S. Aubry and G.P. Tsironis, *Phys. Rev. Lett.* **77**, 4776 (1996).
- [49] J.L. Marín *et al*, *Phys. Rev E* **63**, 066603 (2001).
- [50] P.J. Martínez *et al*, *Chaos* **13**, 610 (2003).
- [51] M. Meister and L.M. Floría, *Eur. Phys. J. B* **37**, 213-221 (2004).
- [52] M. Oster, Master thesis. Linköping University (2002).
- [53] D.N. Christodoulides and E.D. Eugenieva, *Phys. Rev. Lett.* **87**, 233901 (2001).